Contents lists available at ScienceDirect

Environmental Research

journal homepage: www.elsevier.com/locate/envres

Ferroptosis mediated by the interaction between Mfn2 and IREα promotes arsenic-induced nonalcoholic steatohepatitis

Sen Wei[a,1], Tianming Qiu[a,1], Ningning Wang[b,1], Xiaofeng Yao[a], Liping Jiang[c], Xue Jia[a], Ye Tao[a], Jingyuan Zhang[a], Yuhan Zhu[a], Guang Yang[b], Xiaofang Liu[b], Shuang Liu[a], Xiance Sun[a,d,*]

[a] Department of Occupational and Environmental Health, Dalian Medical University, 9 Lvshun South Road, Dalian, 116044, PR China
[b] Department of Nutrition and Food Hygiene, Dalian Medical University, 9 Lvshun South Road, Dalian, 116044, PR China
[c] Experimental Teaching Center of Public Health, Dalian Medical University, 9 Lvshun South Road, Dalian, 116044, PR China
[d] Global Health Research Center, Dalian Medical University, 9 Lvshun South Road, Dalian, 116044, PR China

ARTICLE INFO

Keywords:
Arsenic
Ferroptosis
NASH
ACSL4

ABSTRACT

Exposure to arsenic is a risk factor for nonalcoholic steatohepatitis (NASH). Ferroptosis is a form of regulated cell death defined by the accumulation of lipid peroxidation. In the current study, we observed the occurrence of ferroptosis in arsenic-induced NASH by assessing ferroptosis related hallmarks. *In vitro*, we found that ferrostatin-1 effectively attenuated the executing of ferroptosis and NASH. Simultaneously, the expression of ACSL4 (acyl-CoA synthetase long-chain family member 4) was upregulated in rat's liver and L-02 cells exposed to arsenic. While, suppression of ACSL4 with rosiglitazone or ACSL4 siRNA remarkably alleviated arsenic-induced NASH and ferroptosis through diminishing 5-hydroxyeicosatetraenoic acid (5-HETE) content. Additionally, Mitofusin 2 (Mfn2), a physical tether between endoplasmic reticulum and mitochondria, has rarely been explored in the ferroptosis. Using Mfn2 siRNA or inositol-requiring enzyme 1 alpha (IRE1α) inhibitor, we found NASH and ferroptosis were obviously mitigated through reducing 5-HETE content. Importantly, Co-IP assay indicated that Mfn2 could interact with IRE1α and promoted the production of 5-HETE, ultimately led to ferroptosis and NASH. Collectively, our data showed that ferroptosis is involved in arsenic-induced NASH. These data provide insightful viewpoints into the mechanism of arsenic-induced NASH.

1. Introduction

Arsenic is a natural metalloid element that is discovered extensively in foods, soil and water (Medina-Pizzali et al., 2018). It is reported that more than 200 million people in Bangladesh, Chile, China and the United States are exposed to arsenic through underground water contamination (Hasibuzzaman et al., 2017; Nardone et al., 2017; Wang et al., 2017a; Sorg et al., 2014). There is growing evidence that exposure to arsenic is closely associated with detrimental health influences and soar threats of various diseases, including skin and lung

that NASH plays a paramount regulation in the development of NAFLD is widely acknowledged. At present, studies have indicated that the inflammation response and lipid accumulation are major regulators in the progression of NASH (Ganz and Szabo, 2013). Arsenic-caused NASH has been increasingly studied, but the underlying mechanism is not completely elucidated. Our previous research has found that taurine alleviates arsenic-induced pyroptosis and NASH by suppression of the autophagic-inflammasomal pathway rather than reducing lipid accumulation (Qiu et al., 2018). Furthermore, Wang et al. have demonstrated that apoptosis can effectively regulate the process of NASH in mice and nonhuman primates (Wang et al., 2017b). Therefore, the types of cell damage involved in the process of arsenic-induced NASH are of great concern. Ferroptosis is a newly identified form of the regulated cell death (RCD) and whether it is involved in arsenic-caused NASH is not certain.

Ferroptosis is a non-apoptotic and caspase-independent RCD induced by lipid peroxidation in an iron-dependent manner (Stockwell et al., 2017; Dixon et al., 2012). Some small molecules were identified as a classic inducer of ferroptosis such as erastin and RSL3[16, 17]. It is widely acknowledged that ferroptosis is characterized by three essential hallmarks, containing the loss of glutathione peroxidase 4 (GPX4) activity, the content of available iron and loss of lipid peroxidation repair ability (Dixon and Stockwell, 2019). Although a variety of biological reactions such as iron metabolism, amino acid metabolism and lipid metabolism can affect the sensitivity of ferroptosis (Stockwell et al., 2017), the relationship between lipid metabolism disorder in arsenic-induced NASH and ferroptotic cell death remains deficiently elucidated.

The oxidation of polyunsaturated fatty acids (PUFAs) (e.g., arachidonate, 5-hydroxyeicosatetraenoic acid, 5-HETE) is indispensable for the execution of ferroptosis in response to numerous inducements (Kagan et al., 2017; Wenzel et al., 2017). The free PUFAs are the substrate for phospholipids synthesis of cell membrane and they are esterified and oxidized into ferroptotic signals which are regulated by diverse enzymes. Acyl-CoA synthetase long-chain family (ACSL), as a crucial enzyme in lipid metabolism, is derived from endoplasmic reticulum (ER) and mitochondrial membrane, containing five subtypes of ACSL1, ACSL3, ACSL4, ACSL5, and ACSL6 in brain, liver, and kidney tissues (Chen et al., 2016), yet only ACSL4 has been recognized as a crucial regulator of ferroptosis (Doll et al., 2017). So far, the role of ACSL4 has rarely been explored in arsenic-caused NASH diseases. Therefore, the role and significance of ACSL4 and 5-HETE and their interrelation with ferroptosis in arsenic-induced NASH need to be thoroughly investigated.

In addition, the ER is an organelle that exerts a vital regulator in the process of lipid metabolism, protein synthesis, and cellular calcium storage. In recent studies, ER has been identified as an important regulator in the executing of ferroptosis via protein kinase-like ER kinase (PERK) pathway (Lee et al., 2018; Dixon et al., 2014). Furthermore, Shan (Shan et al., 2017) and Bujisic (Bujisic and Martinon, 2017) et al. both found that inositol-requiring enzyme 1 alpha (IRE1α), one of ER stress signaling pathways, suppressed inflammation response and balanced energy metabolism in the obesity murine model. However, whether IRE1α mediates the initiation of ferroptosis in NASH is still unclear.

Mitofusin-2 (Mfn2) is a GTPase that is involved in the construction of ER-mitochondrial junction (Be Brito and Scorrano, 2008). It has been indicated that ER-mitochondrial junction regulates mitochondrial morphology, intracellular organelle Ca^{2+} exchange, and lipid transport through Mfn2. A growing body of evidence have suggested that mitochondria are closely related to ferroptosis (Neitemeier et al., 2017). Whereas, whether Mfn2 regulates the executing of ferroptosis remains unknown.

In this study, we assumed that ferroptosis was involved in NASH caused by arsenic and that the activation of ACSL4 contributed to ferroptosis through 5-HETE. Additionally, our data found that suppression of ferroptosis was a crucial mechanism protecting against NASH through inhibiting Mfn2/IRE1α-ACSL4 pathway. We aim to provide a new viewpoint and target for the treatment of arsenic-induced NASH.

2. Materials and methods

2.1. Rat model of NASH and ferroptosis

Adult male Sprague-Dawley rats (300 g–350 g, specific pathogen free) were obtained from Institute of Genome Engineered Animal Models for Human Disease of Dalian Medical University (Dalian, China). To explore the influence of $NaAsO_2$ (CAS No.7784-46-5, Sigma-Aldrich, USA) on the liver, the rats were subjected to $NaAsO_2$ at the dosage of 0, 2.5, and 5 mg/kg by gavage for 9 months. The control group was gavaged with distilled water as vehicle. All procedures were performed based on Institutional Animal Care Guidelines and confirmed by the Animal Ethics Committee of Dalian Medical University, the institute issued the permit (Number: [SCXK (liao) 2015e2003]) to this animal study.

2.2. Cell culture

L-02 cells were attained from the China Cell Culture Center (Shanghai, China). The cells were cultured in RPMI 1640 supplemented with 10% fetal bovine serum (Hyclone, USA), antibiotics (HYC-SV30010, Hyclone, USA) and 1% glutamine (G3126, Sigma, USA) under a humidified incubator containing 5% CO_2 at 37 ˚C. To prepare a stock solution (4 mM), 0.52 mg of $NaAsO_2$ was dissolved in 1 mL of phosphate buffered saline (PBS). The L-02 cells were exposed to 0 or 4 μM $NaAsO_2$ for 24 h.

2.3. Inhibitor treatment

Before treatment with $NaAsO_2$, cells were pretreatment with 10 μM ferroptosis specific inhibitor ferrostatin-1 (Fer-1) (SML0583, Sigma-Aldrich, USA), or 50 μM IRE1α inhibitor Irestatin 9389 (1656, Axon Medchem, Holland), or 100 μM Rosiglitazone (ROSI) (S2556, Selleck, USA) for 4 h.

2.4. Cell viability assay

The cytotoxicity of $NaAsO_2$ to the L-02 cells was measured by the Cell Counting Kit-8 (CCK8, CK04, Japan) assay. In brief, the reagent was diluted to the working concentration and added to a 96-well plate (Guangzhou Jet Bio-Filtration Co., Ltd.) planted with L-02 cells for 1 h at 37 ˚C. The cell viability was counted by the absorbance at 450 nm wavelength.

2.5. Iron content detection

The serum iron and non-heme iron level in liver tissue were measured by colorimetric assay kit according to the manufacturer's instructions (A039–1 and A039-2, Nanjing Jincheng Bioengineering Institute, China).

2.6. Transmission electron microscopy (TEM)

The ultrastructure of ER and mitochondria from rat liver tissue was observed by TEM. Slice preparation and electron micrographs taking were conducted as previously described (Wei et al., 2019).

2.7. Glutathione (GSH), malondialdehyde (MDA) content detection

The levels of GSH and MDA from rat liver tissue and cell lysate were measured by colorimetric kits according to the manufacturer's instruction (A006–2 and A003-1, Nanjing Jiancheng Bioengineering Institute, China).

2.8. Lipid reactive oxygen species (ROS) content detection

Lipid ROS was detected using a live cell assay reagent BODIPY 581/591 C11 (D3861, Invitrogen, USA). Cells were incubated with the kit reagent for 30 min at working concentration of 5 μM in the 37 ˚C, and images were obtained with the fluorescence microscope (Olympus BX63, Japan).

2.9. Transient transfection

To explore the role of Mfn2 and ACSL4 in $NaAsO_2$-induced ferroptosis, siRNA was applied to suppress the expression of Mfn2 and ACSL4 in L-02 cells. The siRNA sequences were provided in Supporting Table S1. Transfections were executed using Lipofectamine™ 3000 (L3000008, Invitrogen, USA) according to the manufacturer's protocol.

2.10. Co-immunoprecipitation (Co-IP) assay

L-02 cells were lysed with an IP lysis buffer after $NaAsO_2$ treatment. Cell lysates were preprocessed with magnetic bead before incubating with IRE1α antibody (3294 S, CST, USA) or control IgG (B900620, Proteintech, USA) at 4 ˚C overnight. The Co-IP was captured on magnetic bead and researched by Western blot with antibodies against Mfn2 (12186-1-AP, Proteintech, USA) and IRE1α, respectively.

2.11. Quantitative real-time PCR

Total RNA was released from rat liver tissue with RNAiso Plus (9109, Takara, Japan), then cDNA was synthesized using the Evo M-MLV RT Kit with gDNA Clean for qPCR (AG11705, ACCURATE BIOTECHNOLOGY, HUNAN). The analysis of RT-PCR assay was performed using a Rotor-Gene Q instrument (Qiagen, Germany) with SYBR ® Green Premix Pro Taq HS qPCR Kit (AG11701, ACCURATE BIOTECHNOLOGY, HUNAN), according to the manufacturer's instructions. The ΔΔCt method was used to compare the relative expression levels of mRNA. The primers were provided in Supporting Table S2.

2.12. Western blot assay

Total protein from liver tissues and cell sample were extracted with lysis buffer (92,590, Merck Millipore, USA) containing 1 mM phenylmethylsulfonyl fluoride (PMSF) (KGP610, KeyGEN, China), 1 mM protease inhibitor (KGP603, KeyGEN, China) and 1 mM phosphatase inhibitors (KGP602, KeyGEN, China). The concentration of total protein was measured with the BCA Kit (MK164230, Thermo, USA). The primary antibodies were provided for western blotting in Supporting Table S3.

2.13. Oil Red O staining

Frozen sections from rat liver tissue or treated L-02 cells were washed with ice-cold PBS for three times. The slices of tissue or L-02 cells were painted with Oil Red O (KGA329, KeyGEN, China) for 20 min after being dehydrated with gradient sucrose solution. Then, the liver slices or L-02 cells were washed with purified water for three times and scrutinized under a microscope (Olympus BX63, 40 × 10, Japan).

2.14. Triglyceride (TG) content detection

The level of TG in the liver was measured based on glycerol lipase oxidase (GPO-PAP) method using a TG Assay Kit (A110-1, Nanjing Jiancheng Bioengineering Institute, China) according to the manufacturer's instructions.

2.15. Histopathological examination

For the liver histological analysis, rat liver tissues were fixed in 4% paraformaldehyde, embedded in paraffin, and then stained with hematoxylin and eosin (H&E). The results were obtained using microscopic analyses.

2.16. 5-HETE content detection

The 5-HETE content of lysate of cells and liver tissue was measured using a 5-HETE ELISA Kit (CED739Ge, Uscnlife, China).

2.17. IL-1β and IL-18 content detection

The serum IL-1β and IL-18 content were determined using an ELISA Kit (SEA563Ra and SEA064Ra, Uscnlife, China) according to the manufacturer's instructions.

2.18. Statistical analysis

The data was presented as means ± standard deviation (SD) and comparisons between groups were evaluated with SPSS 20.0, with one-way ANOVA or *t*-test. All experiments were performed independently at least three times to verify the results. $P < 0.05$ was considered statistically significant.

3. Results

3.1. Arsenic triggers NASH and ER stress in the rat liver

The influences of $NaAsO_2$ on rat livers were investigated by H&E staining, Oil Red O staining, and Western blot (Fig. 1). As shown in Fig. 1A, the extent of steatosis and lipid accumulation were aggravated in the 5 mg/kg group compared with the control group. Then, real-time qPCR was conducted to explore the effect of $NaAsO_2$ on gene expressions related to liver lipid synthesis (*ACC*, *FAS*, and *SREBP-1c*) and fibrosis (*COL-1*, *CTG-F*, and *TGF-β*), which were obviously dysregulated in 5 mg/kg group compared with untreated group (Fig. 1B and C). The levels of triglyceride also revealed similar change in the 5 mg/kg group (Fig. 1D). Compared with control group, $NaAsO_2$ distinctly aroused the liver protein expression of MPO, TNF-α, IL-6, pro-IL-1β, and IL-1β (Fig. 1E) and systemic and hepatic inflammation, which was observed through serum IL-1β and IL-18 (Fig. F–G). These data demonstrate that $NaAsO_2$ induced NASH in rat.

Additionally, the levels of p-IRE1α and GRP78 in rat livers were up-regulated after treatment with 5 mg/kg $NaAsO_2$ (Fig. 1H). Meanwhile, the ultrastructure of ER became distended after treatment with 5 mg/kg $NaAsO_2$ (Fig. 1I). These findings capture irritative IRE1α branch of ER stress in rat livers after treatment with $NaAsO_2$.

3.2. Arsenic induces ferroptosis in rat liver

It is well accepted that ACSL4, GPX4, and COX-2 are regarded as core and vital regulators in ferroptosis (Xie et al., 2016). Hence, the expression levels of these proteins were detected to explore the sensitivity of ferroptosis in liver tissues after treatment with $NaAsO_2$. As shown in Fig. 2A, the expression of GPX4 was obviously decreased in the 5 mg/kg group, while the positive monitors of ferroptosis ACSL4 and COX-2 were significantly up-regulated in the 5 mg/kg group compared with the untreated group. In addition, $NaAsO_2$-exposed group (5 mg/kg) showed significant accumulation of iron in serum and liver (Fig. 2B and C). Furthermore, the occurrence of lipid peroxidation in the liver was confirmed by markedly increased MDA (Fig. 2D) and 5-HETE content (Fig. 2E), and diminished GSH content (Fig. 2D). Importantly, the Ptgs2 and ACSL4 mRNA levels were increased obviously in the $NaAsO_2$-exposed groups (2.5 mg/kg and 5 mg/kg) (Fig. 2F). TEM

was further applied to explore morphological traits of ferroptosis. As shown in the ultrastructural images (Fig. 2G), rupture of mitochondrial membrane and reduction or disappearance cristae were observed in the liver of $NaAsO_2$-exposed rats. Together, these results suggest that ferroptosis was involved in the model of NASH triggered by $NaAsO_2$.

3.3. Fer-1 ameliorates ferroptosis, inflammation and lipid accumulation triggered by arsenic in L-02 cells

As manifested in Fig. 3A, the toxicological e

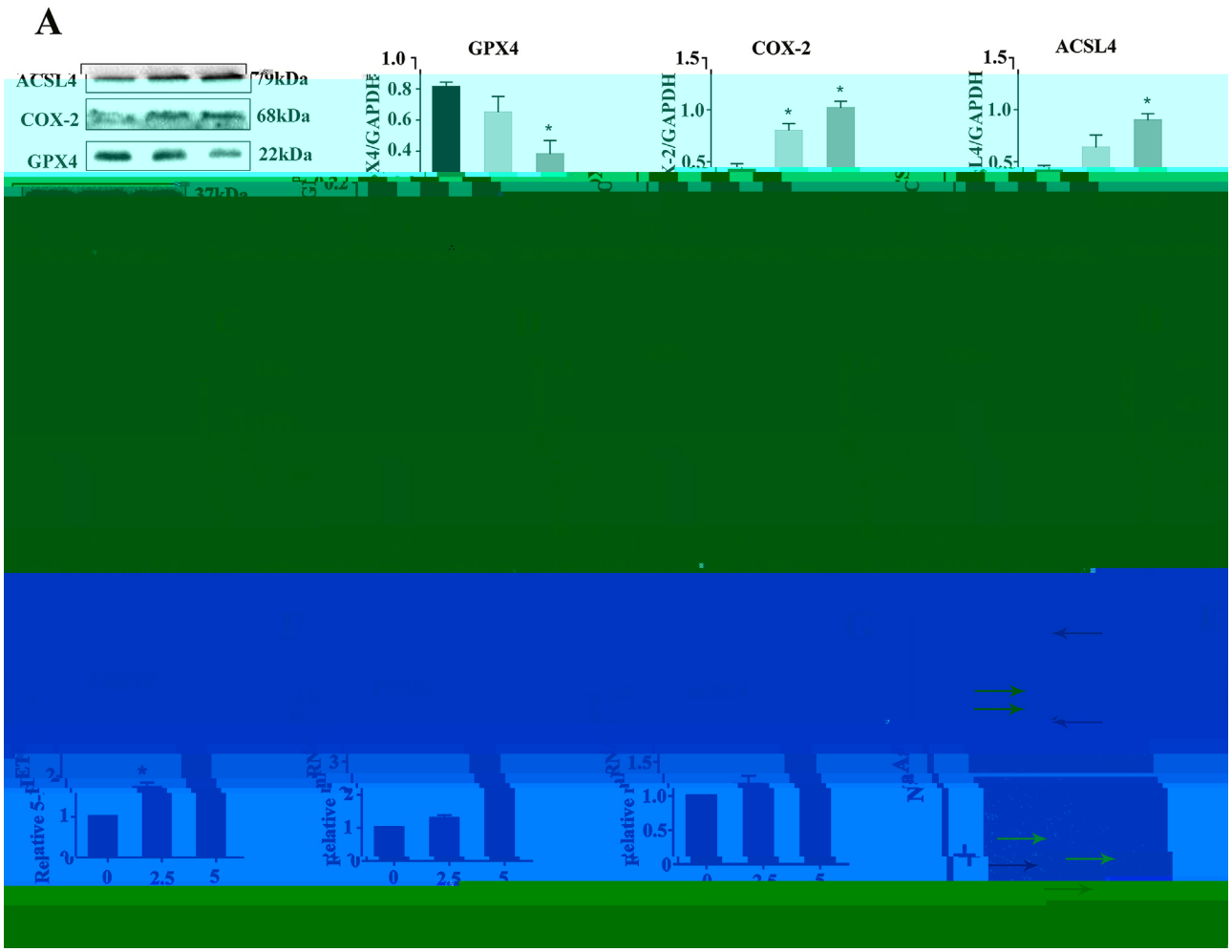

Fig. 2. *Arsenic induces ferroptosis in rat liver.* Male SD rats were subjected to $NaAsO_2$ (0, 2.5 and 5 mg/kg) by gavage for 9 months. (A) The expression of ferroptosis-related proteins following exposure to $NaAsO_2$ (n = 3). (B) Serum iron content, (C) Liver iron content, (D) Relative GSH, MDA content in the liver (n = 6). (E) The 5-HETE content in liver (n = 6). (F) The mRNA expression levels of PTGS2 and ACSL4 genes in liver tissue (n = 6). (G) Ultrastructural features of mitochondria in liver. The red arrow manifest mitochondrial membrane rupture and yellow arrows manifest the decrease or disappearance of mitochondrial cristae (scale bar = 500 nm). All data are expressed as the mean ± SD. $^*P < 0.05$, $^{**}P < 0.001$ vs. control group.

$NaAsO_2$ (4 μM) for 24 h. Fer-1 effectively reduced the cell death surveyed in the CCK8 assay (Fig. 3B). Meanwhile, Fer-1 up-regulated the protein expression of GPX4 and decreased COX-2 protein levels, respectively (Fig. 3C). Furthermore, the depletion of GSH and excess of MDA stimulated by $NaAsO_2$ were significantly improved through pre-processing with Fer-1 (Fig. 3D). Interestingly, Fer-1 also vastly ameliorated the mitochondrial morphology destructed by $NaAsO_2$ (Fig. 3E). Additionally, Fer-1 clearly reduced lipid ROS accumulation evidenced by the green fluorescence intensity with BODIPY 581/591 C11 staining (Fig. 3F). Meanwhile, Fer-1 greatly reduced the protein expression of TNF-α, IL-6, pro-IL-1β, and IL-1β under $NaAsO_2$ stress (Fig. 3G). As shown by Oil Red O staining in Fig. 3H, the $NaAsO_2$-caused lipid droplets deposition was effectively improved by Fer-1.

Collectively, our data verify the involvement of ferroptosis in NASH, and inhibiting ferroptosis could alleviate pathological lesions of NASH.

3.4. Inhibition of ACSL4 suppresses ferroptosis, inflammation and lipid accumulation triggered by arsenic

As a significant elevation of ACSL4 was discovered in liver tissues of rats suffered from 5 mg/kg $NaAsO_2$ (Fig. 2A), the role of ACSL4 in ferroptosis-related NASH deserved to be explored. Hence, we applied ROSI, the pharmacological inhibitor of ACSL4, and ACSL4 siRNA in vitro. After pre-treatment with ROSI (100 μM, 4 h) or ACSL4 siRNA in $NaAsO_2$-exposed L-02 cells, the cell survival under the circumstance of $NaAsO_2$ was notably improved, as showed by CCK8 assay (Figs. 4A and 5A). And the expression of ACSL4 was markedly reduced (Fig. 4B). ACSL4 siRNA obviously decreased the expression of ACSL4 (Fig. S1A). Additionally, ROSI or ACSL4 siRNA reinstated the conveying of GPX4 and reduced COX-2 expression (Figs. 4B and 5B). The abnormal content of GSH and MDA were also effectively reversed by ROSI or ACSL4 siRNA under $NaAsO_2$ stress (Figs. 4C and 5C). Of note, ROSI and ACSL4 siRNA both mitigated the lipid peroxidation reflected by the reduced concentration of 5-HETE and lipid ROS (Fig. 4D and E, 5D-E). Moreover, the expression of inflammatory proteins and excessive lipid accumulation triggered by $NaAsO_2$ were both improved vastly by ROSI or ACSL4 siRNA (Fig. 4F and G, 5 F-G). Together, these data indicate that arsenic-induced ferroptosis and NASH could be retarded by inhibition of ACSL4.

3.5. Arsenic activates ferroptosis, inflammation and lipid accumulation via IRE1α pathway

In vivo, we have found that the expression of IRE1α was distinctly increased in the liver after $NaAsO_2$ exposure (Fig. 1I). To corroborate whether IRE1α adjusted evolution of ferroptosis and NASH, the potent inhibitor of IRE1α, Irestatin9389 was applied. Pre-treatment of the cells with Irestatin9389 (50 μM, 4 h), strongly improved cell survival

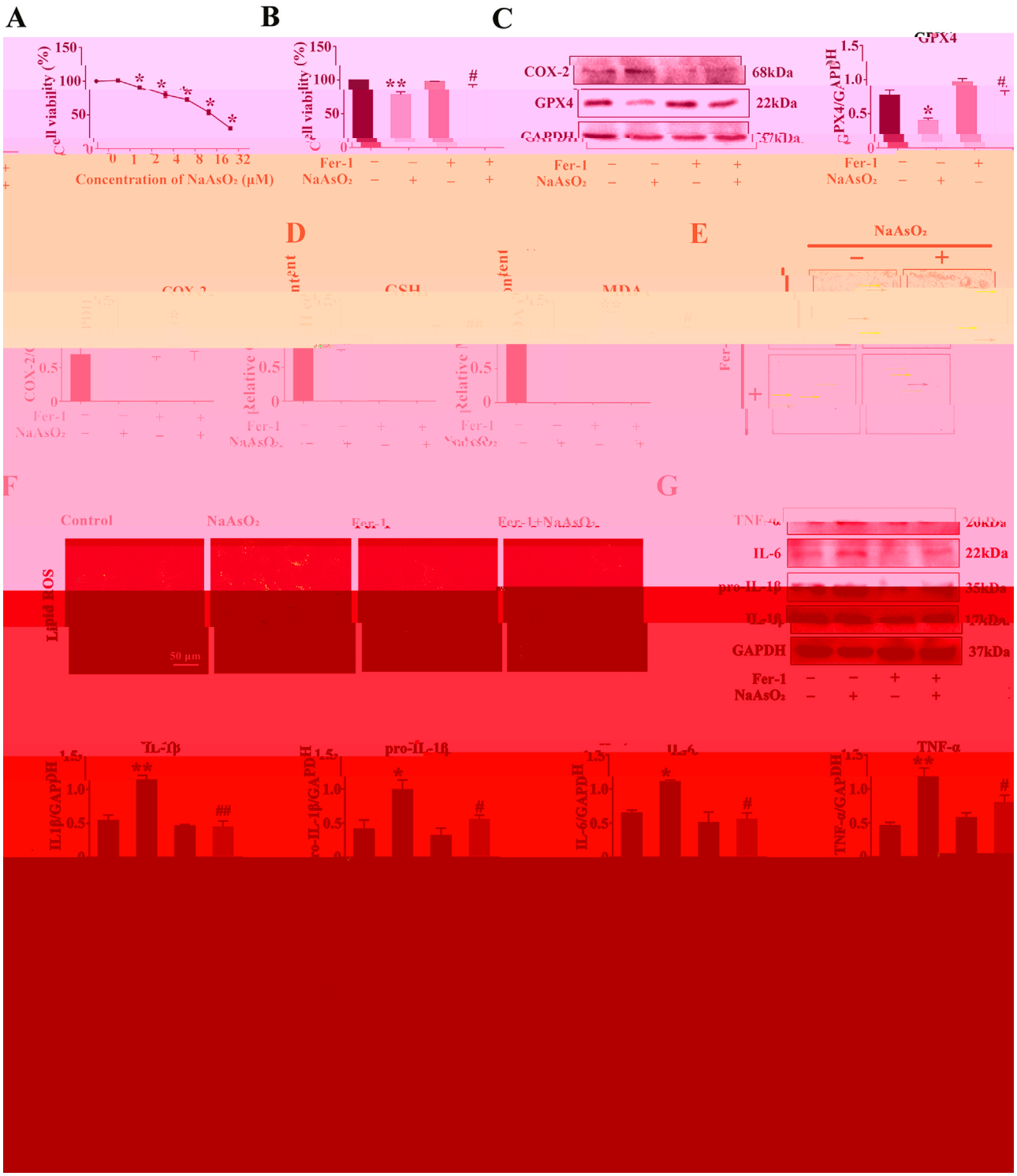

Fig. 3. Fer-1 ameliorates ferroptosis, inflammation and lipid accumulation triggered by arsenic in L-02 cells. (A) The effect of $NaAsO_2$ on L-02 cell viability (n = 6). The L-02 cells were pretreatment with Fer-1 (10 μM, 4 H) before $NaAsO_2$ (4 μM, 24 H) stress. (B) Cell viability in L-02 cells (n = 6). (C) The expression of ferroptosis-related proteins following exposure to $NaAsO_2$ (n = 3). (D) Effects of $NaAsO_2$ and Fer-1 on relative GSH and MDA content in L-02 cells. (E) Ultrastructural features of mitochondria in liver. The red arrow manifest mitochondrial membrane rupture and yellow arrows manifest the decrease or disappearance of mitochondrial cristae (scale bar = 500 nm). (F) Cell lipid ROS was measured by BODIPY 581/591 C11 staining (scale bar = 50 μm). (G) The expression of inflammation-related proteins following exposure to $NaAsO_2$ (n = 3). (H) Effects of Fer-1 on $NaAsO_2$-induced lipid accumulation (scale bar = 50 μm, n = 3). All data are expressed as the mean ± SD, n = 3. $^{*}P < 0.05$, $^{**}P < 0.001$ vs. control group, $\#P < 0.05$, $\#\#P < 0.001$ vs. $NaAsO_2$ group.

(Fig. 6A), restored GPX4 protein expression and reduced COX-2 protein content compared to $NaAsO_2$-exposed group (Fig. 6B). Furthermore, the concentration of GSH obviously soared and MDA content dropped after pretreatment with Irestatin9389 (Fig. 6C). Additionally, Irestatin9389 decreased lipid peroxidation manifested as the lessened level of green fluorescence (BODIPY 581/591 C11) (Fig. 6D), and 5-HETE (Fig. 6E). Furthermore, the protein expressions of TNF-α, IL-6, pro-IL-1β, and IL-1β enhanced by $NaAsO_2$ were decreased by Irestatin9389 (Fig. 6F).

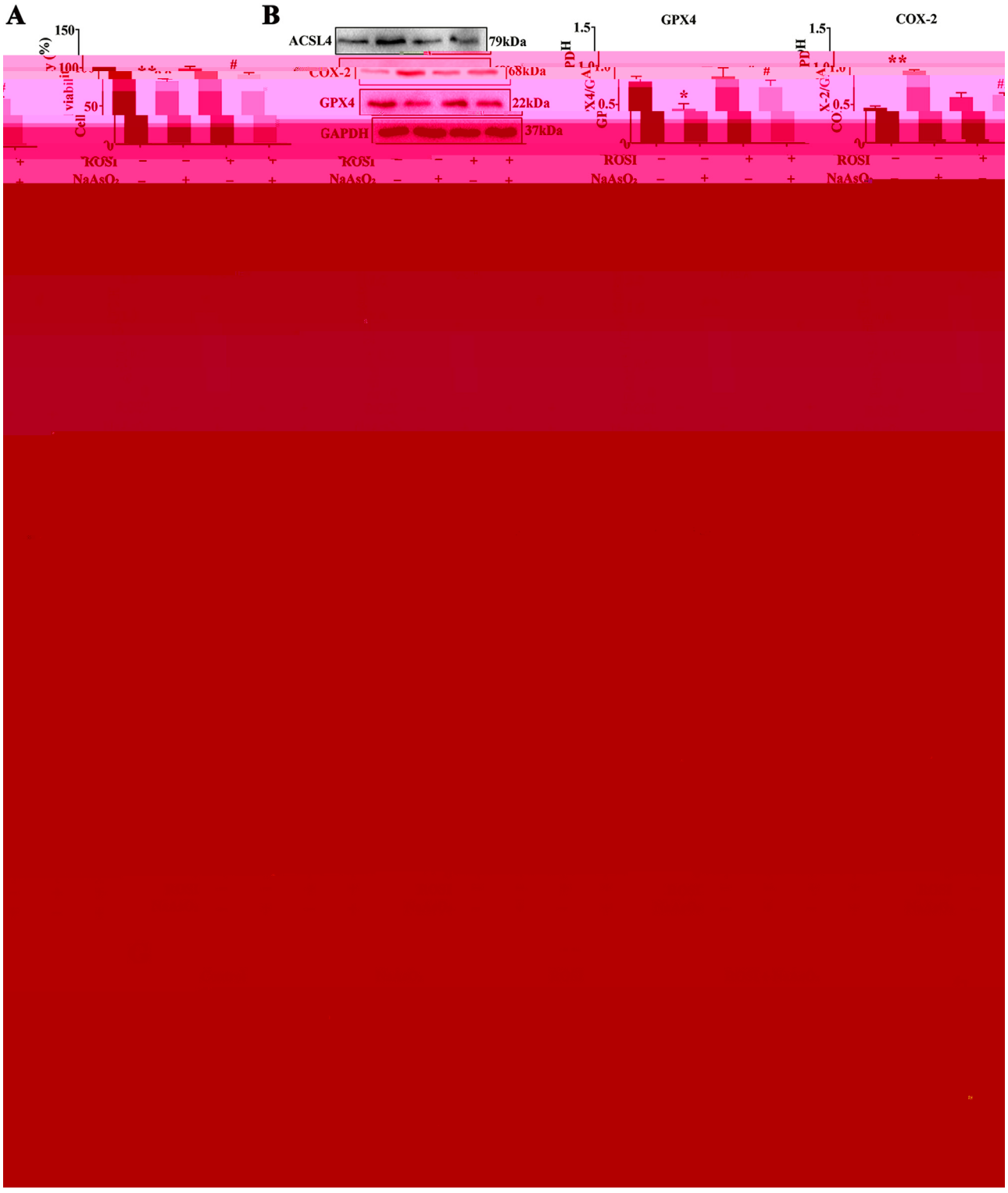

Fig. 4. Pharmacological inhibitor of ACSL4 suppresses ferroptosis, inflammation and lipid accumulation triggered by arsenic. The L-02 cells were pretreatment with ROSI (100 αω

Intriguingly, the up-regulated ACSL4 induced by $NaAsO_2$ was restored by Irestatin9389 (Fig. 6G). Meanwhile, the lipid accumulation was effectively ameliorated by Irestatin9389 compared with $NaAsO_2$ group (Fig. 6H). Taken together, our data indicate that $NaAsO_2$ evoked ferroptosis and NASH via IRE1α pathway.

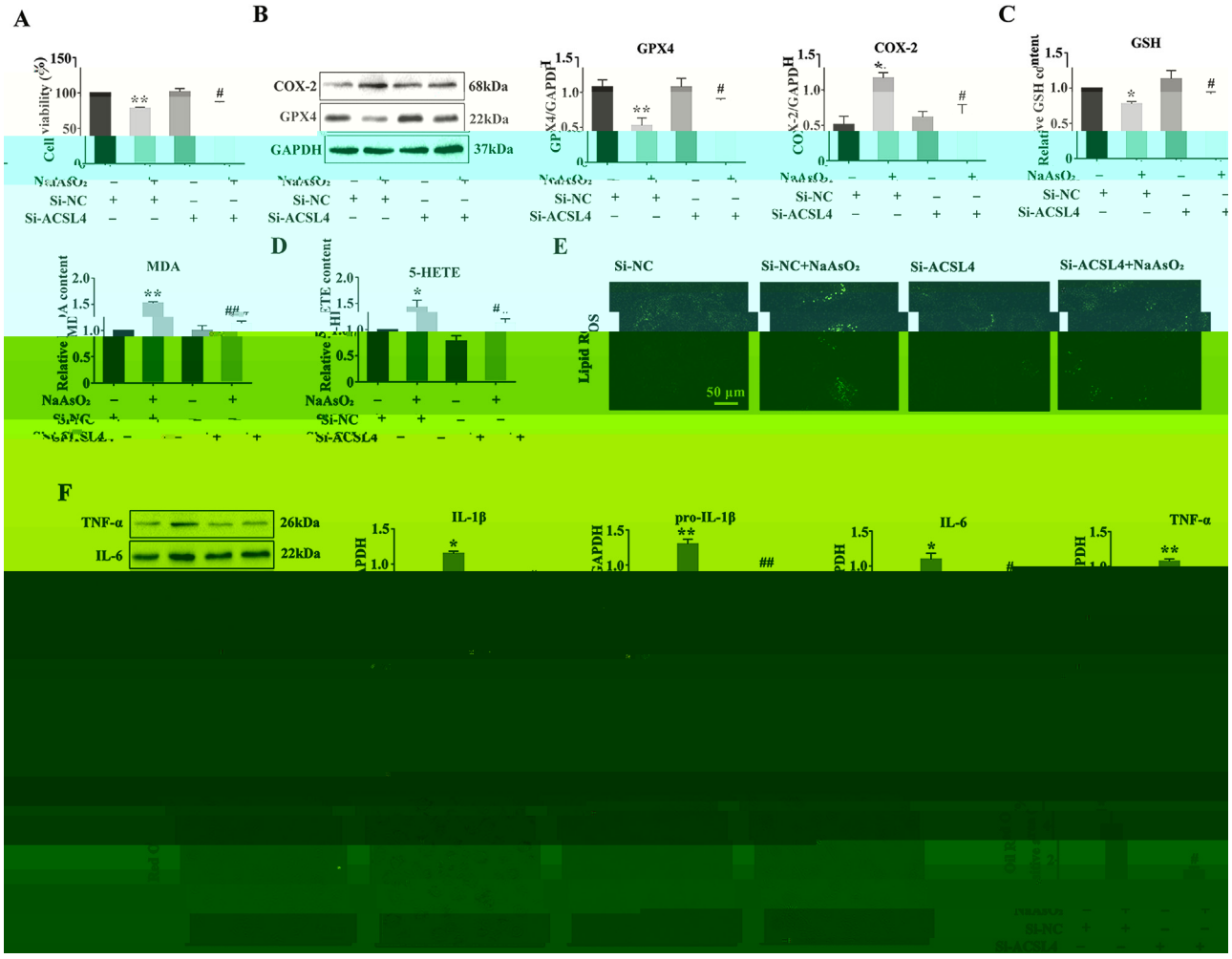

Fig. 5. Knock-down of ACSL4 suppresses ferroptosis, inflammation and lipid accumulation triggered by arsenic. The L-02 cells were transfected with Si-NC or Si-ACSL4 for 1 days before $NaAsO_2$ (4 μM, 24 H) treatment. (A) Cell viability in L-02 cells (n = 6). (B) The expression of GPX4 and COX-2 following exposure to $NaAsO_2$ (n = 3). (C) Effects of $NaAsO_2$ and Si-ACSL4 on relative GSH and MDA content. (D) Effects of $NaAsO_2$ and Si-ACSL4 on 5-HETE content (n = 6). (E) Cell lipid ROS was detected by BODIPY 581/591 C11 staining (scale bar = 50 μm). (F) The expression of inflammation-related proteins following exposure to $NaAsO_2$ (n = 3). (G) Effects of Si-ACSL4 on $NaAsO_2$-induced lipid accumulation (scale bar = 50 μm, n = 3). All data are expressed as the mean ± SD, n = 3. $^*P < 0.05$, $^{**}P < 0.001$ vs. control group, $\#P < 0.05$, $\#\#P < 0.001$ vs. $NaAsO_2$ group.

3.6. Arsenic induces ferroptosis, inflammation and lipid accumulation through interacting Mfn2 with IRE1α

According to previous studies, the pivotal role of mitochondria in the process of ferroptosis has been well confirmed (Gao et al., 2019). However, it is unclear whether outer mitochondrial membrane Mfn2 was involved in the executing of ferroptosis. As manifested in Fig. S2A, Mfn2 siRNA prominently abolished the expression of Mfn2. Then, Mfn2 siRNA was proved to attenuate the toxicity of $NaAsO_2$ on L-02 cells (Fig. 7A). Simultaneously, Mfn2 siRNA regained GPX4 expression and decreased COX-2 expression (Fig. 7B), recovered GSH content and reduced MDA concentration (Fig. 7C). Additionally, $NaAsO_2$-induced augment of lipid ROS and 5-HETE content were apparently inhibited by Mfn2 siRNA (Fig. 7D and E). Moreover, the excessive lipid deposition and over-production of inflammatory proteins prompted by $NaAsO_2$ were also down-regulated after treatment with Mfn2 siRNA (Fig. 7F and G). Thus, Mfn2 appeared to act as a driving role in the evolution of ferroptosis and NASH induced by $NaAsO_2$.

Based on the above data, Mfn2 and IRE1α were proved to be involved in the executing of $NaAsO_2$-caused ferroptosis and NASH. To further explore the regulatory mechanism of the effects of Mfn2 and IRE1α in the process of ferroptosis and NASH, Co-IP experiment was conducted. As manifested in Fig. 7H, our results indicate for the first time that Mfn2 could combine with IRE1α, which provoked ferroptosis and NASH induced by $NaAsO_2$.

4. Discussion

In the present study, our data indicated that $NaAsO_2$ led to ER stress, and upregulated ACSL4 expression and 5-HETE, ultimately induced ferroptotic cell death and NASH. Mechanistically, we showed that $NaAsO_2$-caused ferroptotic cell death relied on the combination of Mfn2 with IRE1α via manipulating the production of 5-HETE. Furthermore, inflammatory response and abnormal lipid accumulation of NASH were obviously improved through suppression of the Mfn2/IRE1α-ACSL4 pathway.

RCD, which includes apoptosis, necrosis, and autophagy, is a pivotal molecular process for the cell development and differentiation, reproduction, and homeostasis (Napoletano et al., 2019; Thompson, 1995; Behrends et al., 2010). Recently, Stockwell et al. firstly identified a new form of RCD called ferroptosis (Cao and Dixon, 2016). The ferroptotic cell death is defined as overpowering lipid ROS depended upon iron overload, which is intimately associated with diverse human diseases. Excess iron content, PUFAs, ferroptosis related proteins and a reduction in antioxidants are essential for the executing of ferroptosis. Given that PUFAs are strictly adjusted in order to sustain cellular

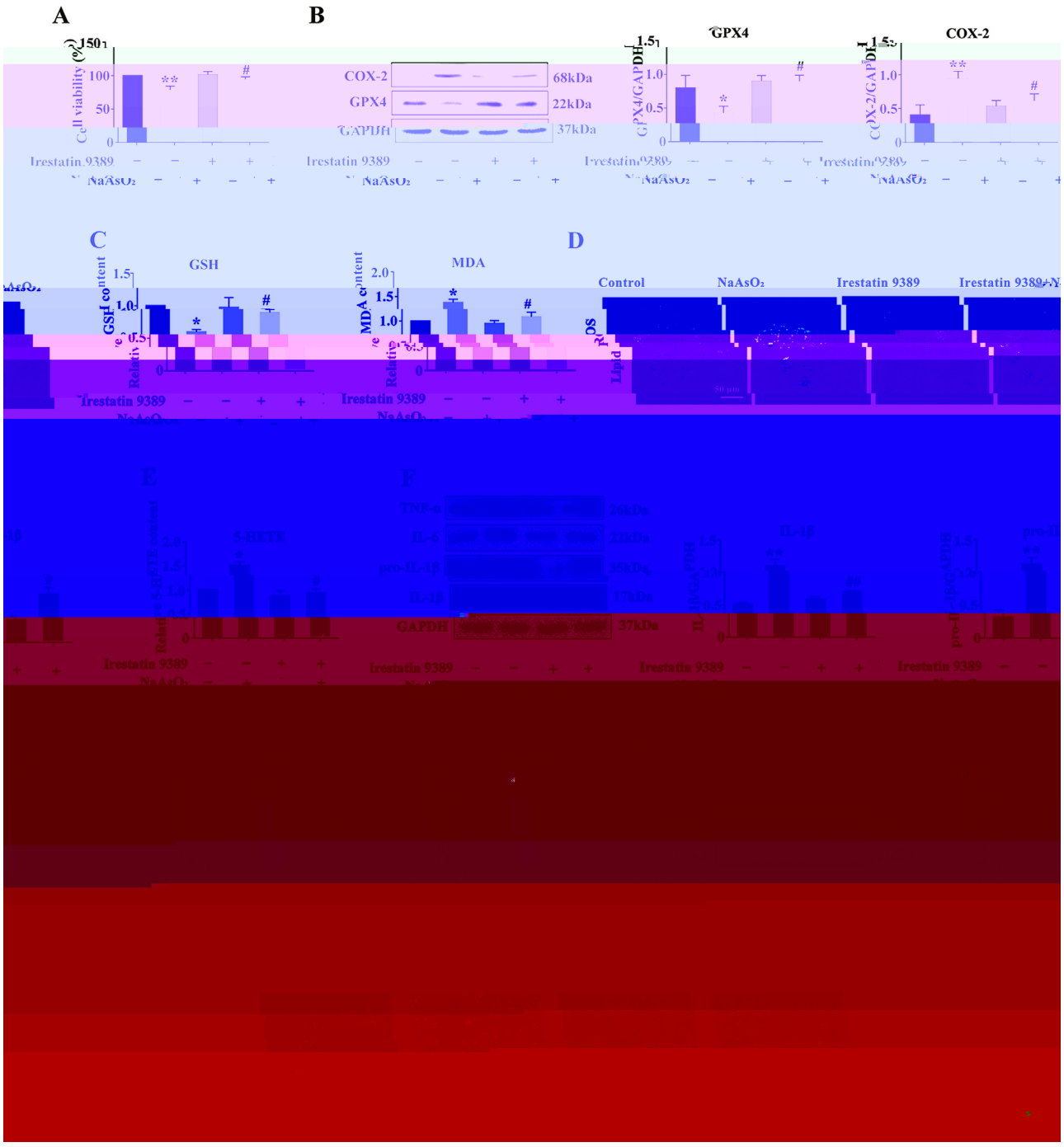

Fig. 6. Arsenic activates ferroptosis, inflammation and lipid accumulation via IRE1α pathway. The L-02 cells were pretreatment with irestatin9389 (50 μM, 4 H) before $NaAsO_2$ (4 μM, 24 H) treatment. (A) Cell viability in L-02 cells (n = 6). (B) The expression of GPX4 and COX-2 following exposure to $NaAsO_2$ (n = 3). (C) Effects of $NaAsO_2$ and irestatin9389 on relative GSH and MDA content in L-02 cells. (D) Cell lipid ROS was measured by BODIPY 581/591 C11 staining (scale bar = 50 μm). (E) Effects of $NaAsO_2$ and irestatin9389 on 5-HETE content (n = 6). (F) The expression of inflammation-related proteins following exposure to $NaAsO_2$ (n = 3). (G) Effects of $NaAsO_2$ and irestatin9389 on ACSL4 expression (n = 3). (H) Effects of irestatin9389 on $NaAsO_2$-induced lipid accumulation (scale bar = 50 μm, n = 3). All data are expressed as the mean ± SD, n = 3. $^*P < 0.05$, $^{**}P < 0.001$ vs. control group, $\#P < 0.05$, $\#\#P < 0.001$ vs. $NaAsO_2$ group.

function, it is not amazed that abnormal oxidation of PUFAs induces a batch of diseases, including ischemia/reperfusion injury (Li et al., 2019a). Intriguingly, it is well accepted that two main regulators of NASH are inflammatory response and anomalous lipid accumulation (Mansouri et al., 2018). Hence, we assumed that ferroptosis might be a vital process accelerating the occurrence of NASH.

To verify the presumptive role of ferroptosis in the process of NASH, we represented ferroptosis in a rat model of NASH. The animal model of NASH was established after $NaAsO_2$ average for 9 months, evidenced by histomorphology of fibrosis and lipid droplet deposition, overexpression of inflammatory proteins, upregulation of lipid synthesis- and fibrosis-related genes, and high hepatic TG content. To confirm the existence of ferroptosis in $NaAsO_2$-caused NASH, we monitored the correlative hallmarks of ferroptosis, including the GSH and MDA content, GPX4 and COX-2 protein expression, PTGS2 mRNA levels in the liver, iron levels in serum and liver tissue and mitochondrial morphology in liver tissues. In general, these data indicate that ferroptosis is strongly associated with NASH induced by $NaAsO_2$, which is

Fig. 7. Arsenic induces ferroptosis, inflammation and lipid accumulation through interacting Mfn2 with IRE1α. The L-02 cells were transfected with Si-NC or Si-Mfn2 for 1 days before $NaAsO_2$ (4 μM, 24 H) treatment. (A) Cell viability in L-02 cells (n = 6). (B) The expression of GPX4 and COX-2 following exposure to $NaAsO_2$ (n = 3). (C) Effects of $NaAsO_2$ and Si-Mfn2 on relative GSH and MDA content. (D) Cell lipid ROS was detected by BODIPY 581/591 C11 staining (scale bar = 50 μm). (E) Effects of $NaAsO_2$ and Si-Mfn2 on 5-HETE content (n = 6). (F) Effects of Si-Mfn2 on $NaAsO_2$-induced lipid accumulation (scale bar = 50 μm, n = 3). (G) The expression of inflammation-related proteins following exposure to $NaAsO_2$ (n = 3). (H) To confirm the interacting of Mfn2 and IRE1α, Co-IP assay was performed. All data are expressed as the mean ± SD, n = 3. $*P < 0.05$, $**P < 0.001$ vs. control group, $\#P < 0.05$, $\#\#P < 0.001$ vs. $NaAsO_2$ group.

consistent with findings of Tsurusaki et al. (2019).

Recently, Wu et al. found that pharmacological targeting or knockout of ACSL4 is a feasible therapeutic approach against the executing of ferroptosis (Wu et al., 2019). In addition, ACSL4 aggregates cellular membranes with long polyunsaturated ω6 fatty acids, and losing of ACSL4 up-regulated resistance to ferroptosis (Dixon et al., 2015). Mechanistically, PUFAs can be oxidized into hydroxyeicosatetraenoic acids (e.g., 5-HETE) by ACSL4 during the procedure of ferroptosis. Furthermore, Yuan et al. have found that ACSL4 acts as a crucial regulator in the process of erastin triggered ferroptosis via 5-HETE-modulated lipotoxicity (Lee et al., 2018), which is consistent with the research by Dixon (Dixon et al., 2014). In our study, ACSL4 expression and 5-HETE level were obviously upregulated in the $NaAsO_2$-induced NASH model in *vivo* and in *vitro*. To explore the role of ACSL4 in NASH triggered by $NaAsO_2$, we applied ROSI or ACSL4 siRNA in L-02 cells, to gain pharmacological or genetic inhibition of ACSL4. Our data revealed that inhibition of ACSL4 eliminated the executing of $NaAsO_2$-triggered ferroptosis, and ameliorated the progression of NASH. Meanwhile, the 5-HETE content was also distinctly down-regulated after suppression of ACSL4. Furthermore, Yuan et al. have suggested that pharmacological suppression of 5-HETE by zileuton can combat with erastin-induced ferroptosis (Yuan et al., 2016; Liu et al., 2015), which is consistent with our research. Taken together, our study uncovers that ACSL4 mediates executing of ferroptosis and NASH via commanding the levels of 5-HETE.

It is generally acknowledged that aberrant ER stress plays a crucial role in the pathological changes of hepatocytes through manipulating abnormal lipid accumulation and inflammatory response, and eventually leads to a series of liver diseases (Lebeaupin et al., 2018). It's also believed that the anomalous accumulation of lipid led by inflammatory response is deemed as a vital driving factor of NASH (Machado and Diehl, 2016). There is growing evidence that overreactive ER stress is closely related to the progression of NASH (Kim et al., 2018; Hernandez-Alvarez et al., 2019). In the current study, we revealed that $NaAsO_2$ motivated NASH and ferroptosis via ER stress-regulated lipid metabolism pathway. Besides, Dixon and Se et al. both have established that erastin triggers ferroptosis and ER stress by virtue of activation of the PERK-eIF2α-ATF4-CHOP pathway (Lee et al., 2018; Dixon et al., 2014). In the previous study, we detected enhanced IREα phosphorylation in INS-1 cells and rat tissues under $NaAsO_2$ stress (Pei et al., 2019). Here in, after the application of the IRE1α inhibitor Irestatin 9389, we found that the 5-HETE level and ACSL4 expression elevated by $NaAsO_2$ were significantly reversed, ultimately improving NASH and ferroptosis. In the present study, we aimed to investigate the influence of lipid metabolism regulated by ER in ferroptosis. IRE1α, an upstream modulator of many pathways, is vital in the ER function. There is also

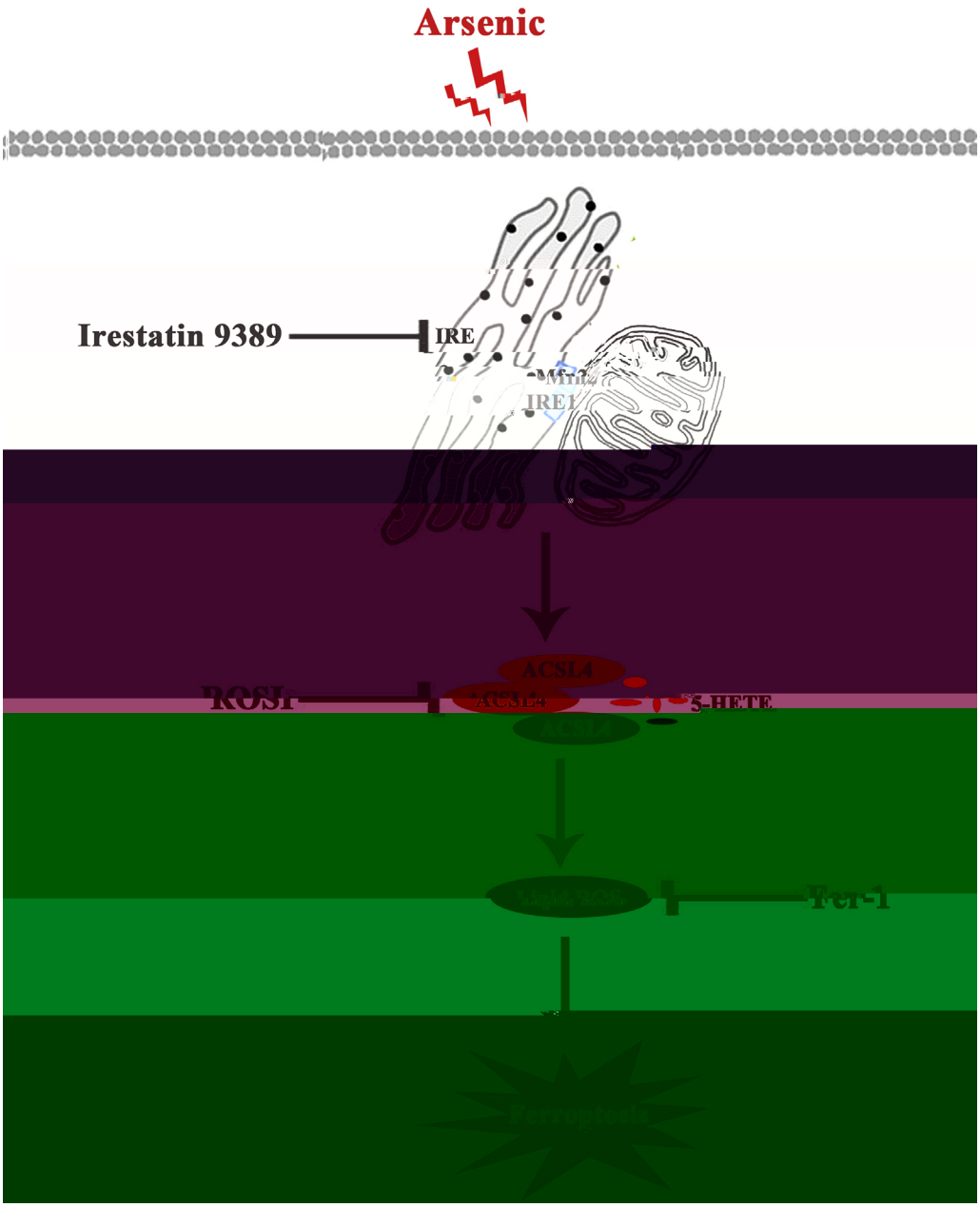

Fig. 8. Arsenic induces rat liver NASH and Ferroptosis via interacting between Mitofusin-2 with IRE1α. $NaAsO_2$ increases IRE1and Mfn2 expression, subsequently led to upregulated ACSL4 expression and 5-HETE via the directly combination Mfn2 with IRE1α, ultimately induced ferroptotic cell death.

evidence that the IRE1α-JNK pathway and IRE1α/XBP-1 activity are indispensable for autophagy activation after ER stress (Muoz et al., 2348). Of course, whether IRE1α, as an upstream regulator, interacts with other proteins to play an important role in $NaAsO_2$-induced ferroptosis is worth further investigation in the future. In a word, our study verifies that IRE1α mediates progression of NASH and ferroptosis via manipulating 5-HETE level.

The role of mitochondria in the ferroptosis is extensively investigated (Abdalkader et al., 2018). Mfn2 is originated from the mitochondrial membrane and the ER surface and has been advocated to be the physical chain between the two organelles (Leal et al., 2016). Thus, the dysfunction of Mfn2 is deemed to be closely associated with human diseases. Meanwhile, Mfn2 content was found to be diminished in mouse models of steatosis or NASH (Gao et al., 2018; Simao et al., 2019), which is inconsistent with our study. In the present study, the expression of Mfn2 in rat liver was up-regulated after $NaAsO_2$ stress, which is consistent with the study by Siwen et al. (Li et al., 2019b). This conclusion may be linked to the hepatotoxicity of arsenic. Many harmful substances have different effects and arsenic is without exception. The molecular mechanism of $NaAsO_2$-mediated Mfn2 expression deserves further investigation.

Mitochondrial fusion and fission are crucial for the maintenance of normal tricarboxylic acid (TCA) cycle and oxidative phosphorylation. Gao et al. have previously found TCA cycle, electron transport chain, and glutaminolysis function are indispensable in the process of cysteine-deprivation-induced ferroptosis (Gao et al., 2019). However, as a crucial regulator of mitochondrial inner membrane fusion, Mfn2 has been poorly surveyed in the executing of ferroptosis. Here, we found Mfn2 content increased in rat model of NASH and ferroptosis. Then we applied Mfn2 siRNA to explore the concrete role of Mfn2 in the process of NASH and ferroptosis. After knockdown of Mfn2, $NaAsO_2$-caused NASH and ferroptosis were effectively mitigated through manipulating 5-HETE level. Moreover, the regulatory effect of Mfn2 on IRE1α leads us to hypothesize that the interaction between Mfn2 and IRE1α may

underly the mechanism of $NaAsO_2$-induced ferroptosis and NASH. In our study, we found that Mfn2 exerted an upstream role in $NaAsO_2$-induced ferroptosis in L-02 cells. In fact, Juan et al. have found that Mfn2 is an upstream regulator of PERK in unfolded protein response (UPR) and mitochondrial function (Muoz et al., 2348), suggesting that Mfn2 has been identified as a possible interacting partner with IRE1α. In the present study, we firstly illuminated the relationship between Mfn2 and IRE1α via Co-IP assay, and found that under $NaAsO_2$ exposure Mfn2 could combine with IRE1α to incur lipid metabolic disorders, which triggered NASH and ferroptosis. However, the exact molecular relationship between Mfn2 and IRE1α in the $NaAsO_2$-caused ferroptosis and NASH is worth exploring in the future study.

In summary, our study demonstrates that ferroptosis is involved in $NaAsO_2$-triggered NASH and leads to liver injury. ACSL4, a potent producer of 5-HETE, is upregulated in NASH and contributes to the lipid metabolism disturbance. Besides, we also indicate that inhibiting ferroptosis improves $NaAsO_2$-induced NASH via suppression of the Mfn2/IRE1α-ACSL4 pathway (Fig. 8). These findings are expected to provide a novel target strategy for $NaAsO_2$-induced NASH and ferroptosis.

Author contribution

S.W., and X.S. designed the studies. S.W., T.Q., Y.T., S.L., and X.J. assisted with animal experiments. S.W., Y.T., L.J., J.Z., Y.Z., G.Y., and X.L., participated in cell experiments. S.W. wrote the manuscript. X.Y., N.W., T.Q., and X.S. revised the manuscript. All authors reviewed the manuscript. X.S. is the guarantor of the article.

Declaration of competing interest

The authors assert that they have on conflict of interest.

Acknowledgments

This study was sponsored by the National Natural Science Foundation of China (NSFC, 81872566).

Appendix A. Supplementary data

Supplementary data to this article can be found online at https://doi.org/10.1016/j.envres.2020.109824.

References

Abdalkader, M., Lampinen, R., Kanninen, K.M., Malm, T.M., Liddell, J.R., 2018. Targeting Nrf2 to suppress ferroptosis and mitochondrial dysfunction in neurodegeneration. Front. Neurosci. 12, 466–478.

Be Brito, O.M., Scorrano, L., 2008. Mitofusin 2 tethers endoplasmic reticulum to mitochondria. Nature 456 (7222), 605–610.

Bedogni, G., Miglioli, L., Masutti, F., Tiribelli, C., Marchesini, G., Bellentani, S., 2005. Prevalence of and risk factors for nonalcoholic fatty liver disease: the Dionysos nutrition and liver study. Hepatology 42 (1), 44–52.

Behrends, C., Sowa, M.E., Gygi, S.P., Harper, J.W., 2010. Network organization of the human autophagy system. Nature 466 (7302), 68–76.

Bujisic, B., Martinon, F., 2017. IRE1 gives weight to obesity-associated inflammation. Nat. Immunol. 18 (5), 479–480.

Cao, J.Y., Dixon, S.J., 2016. Mechanisms of ferroptosis. Cell. Mol. Life Sci. : CM 73 (11–12), 2195–2209.

Castriota, F., Acevedo, J., Ferreccio, C., Smith, A.H., Liaw, J., Smith, M.T., et al., 2018. Obesity and increased susceptibility to arsenic-related type 2 diabetes in Northern Chile. Environ. Res. 167, 248–254.

Chen, W.C., Wang, C.Y., Hung, Y.H., Weng, T.Y., Yen, M.C., Lai, M.D., 2016. Systematic analysis of gene expression alterations and clinical outcomes for long-chain acyl-coenzyme A synthetase family in cancer. PloS One 11 (5) 0155660-0155671.

Dixon, S.J., Stockwell, B.R., 2019. The hallmarks of ferroptosis. Annu. Rev. Cell Biol. 3 (1), 35–54.

Dixon, S.J., Lemberg, K.M., Lamprecht, M.R., Skouta, R., Zaitsev, E.M., Gleason, C.E., et al., 2012. Ferroptosis: an iron-dependent form of nonapoptotic cell death. Cell 149 (5), 1060–1072.

Dixon, S.J., Patel, D.N., Welsch, M., Skouta, R., Lee, E.D., Hayano, M., et al., 2014. Pharmacological inhibition of cystine-glutamate exchange induces endoplasmic reticulum stress and ferroptosis. eLife 3 02523-02548.

Dixon, S.J., Winter, G.E., Musavi, L.S., Lee, E.D., Snijder, B., Rebsamen, M., et al., 2015. Human haploid cell genetics reveals roles for lipid metabolism genes in nonapoptotic cell death. ACS Chem. Biol. 10 (7), 1604–1609.

Doll, S., Proneth, B., Tyurina, Y.Y., Panzilius, E., Kobayashi, S., Ingold, I., et al., 2017. ACSL4 dictates ferroptosis sensitivity by shaping cellular lipid composition. Nat. Chem. Biol. 13 (1), 91–98.

Ganz, M., Szabo, G., 2013. Immune and inflammatory pathways in NASH. Hepatology International 7 (2 Suppl. ment), 771–781.

Gao, W., Du, X., Lei, L., Wang, H., Zhang, M., Wang, Z., et al., 2018. NEFA-induced ROS impaired insulin signalling through the JNK and p38MAPK pathways in non-alcoholic steatohepatitis. J. Cell Mol. Med. 22 (7), 3408–3422.

Gao, M., Yi, J., Zhu, J., Minikes, A.M., Monian, P., Thompson, C.B., et al., 2019. Role of mitochondria in ferroptosis. Mol. Cell 73 (2), 354–363.

Hasibuzzaman, M.M., Hossain, S., Islam, M.S., Rahman, A., Anjum, A., Hossain, F., et al., 2017. Association between arsenic exposure and soluble thrombomodulin: a cross sectional study in Bangladesh. PloS One 12 (4) 0175154-0175161.

Hernandez-Alvarez, M.I., Sebastian, D., Vives, S., Ivanova, S., Bartoccioni, P., Kakimoto, P., et al., 2019. Deficient endoplasmic reticulum-mitochondrial phosphatidylserine transfer causes liver disease. Cell 177 (4), 881–895.

Kagan, V.E., Mao, G., Qu, F., Angeli, J.P., Doll, S., Croix, C.S., et al., 2017. Oxidized arachidonic and adrenic PEs navigate cells to ferroptosis. Nat. Chem. Biol. 13 (1), 81–90.

Kim, J.Y., Garcia-Carbonell, R., Yamachika, S., Zhao, P., Dhar, D., Loomba, R., et al., 2018. ER stress drives lipogenesis and steatohepatitis via caspase-2 activation of S1P. Cell 175 (1), 133–145.

Kuo, C.C., Moon, K.A., Wang, S.L., Silbergeld, E., Navas-Acien, A., 2017. The association of arsenic metabolism with cancer, cardiovascular disease, and diabetes: a systematic review of the epidemiological evidence. Environ. Health Perspect. 125 (8) 087001-087010.

Leal, N.S., Schreiner, B., Pinho, C.M., Filadi, R., Wiehager, B., Karlstrom, H., et al., 2016. Mitofusin-2 knockdown increases ER-mitochondria contact and decreases amyloid beta-peptide production. J. Cell Mol. Med. 20 (9), 1686–1695.

Lebeaupin, C., Vallee, D., Hazari, Y., Hetz, C., Chevet, E., Bailly-Maitre, B., 2018. Endoplasmic reticulum stress signalling and the pathogenesis of non-alcoholic fatty liver disease. J. Hepatol. 69 (4), 927–947.

Lee, Y.S., Lee, D.H., Choudry, H.A., Bartlett, D.L., Lee, Y.J., 2018. Ferroptosis-induced endoplasmic reticulum stress: cross-talk between ferroptosis and apoptosis. Mol. Canc. Res. : MCR 16 (7), 1073–1076.

Li, Y., Feng, D., Wang, Z., Zhao, Y., Sun, R., Tian, D., et al., 2019a. Ischemia-induced ACSL4 activation contributes to ferroptosis-mediated tissue injury in intestinal ischemia/reperfusion. Cell Death Differ. 26 (11), 2284–2299.

Li, S., Zhao, H., Wang, Y., Shao, Y., Liu, J., Xing, M., 2019b. Arsenic-induced cardiotoxicity correlates with mitochondrial damage and trace elements imbalance in broiler chickens. Poultry Sci. 98 (2), 734–744.

Lin, H.J., Sung, T.I., Chen, C.Y., Guo, H.R., 2013. Arsenic levels in drinking water and mortality of liver cancer in Taiwan. J. Hazard Mater. 262, 1132–1138.

Liu, Y., Wang, W., Li, Y., Xiao, Y., Cheng, J., Jia, J., 2015. The 5-lipoxygenase inhibitor zileuton confers neuroprotection against glutamate oxidative damage by inhibiting ferroptosis. Biol. Pharm. Bull. 38 (8), 1234–1239.

Machado, M.V., Diehl, A.M., 2016. Pathogenesis of nonalcoholic steatohepatitis. Gastroenterology 150 (8), 1769–1777.

Mansouri, A., Gattolliat, C.H., Asselah, T., 2018. Mitochondrial dysfunction and signaling in chronic liver diseases. Gastroenterology 155 (3), 629–647.

Medina-Pizzali, M., Robles, P., Mendoza, M., Torres, C., 2018. [Arsenic intake: impact in human nutrition and health]. Rev. Peru. Med. Exp. Salud Pública 35 (1), 93–102.

Muoz JP, Ivanova Sk, Sánchez-Wandelmer J, Martínez-Cristóbal P, Noguera E, Sancho A, et al. Mfn2 modulates the UPR and mitochondrial function via repression of PERK. EMBO J., 32(17): 2348-2361.

Napoletano, F., Baron, O., Vandenabeele, P., Mollereau, B., Fanto, M., 2019. Intersections between regulated cell death and autophagy. Trends Cell Biol. 29 (4), 323–338.

Nardone, A., Ferreccio, C., Acevedo, J., Enanoria, W., Blair, A., Smith, A.H., et al., 2017. The impact of BMI on non-malignant respiratory symptoms and lung function in arsenic exposed adults of Northern Chile. Environ. Res. 158, 710–719.

Neitemeier, S., Jelinek, A., Laino, V., Hoffmann, L., Eisenbach, I., Eying, R., et al., 2017. BID links ferroptosis to mitochondrial cell death pathways. Redox biology 12, 558–570.

Pei, P., Yao, X., Jiang, L., Qiu, T., Wang, N., Yang, L., et al., 2019. Inorganic arsenic induces pyroptosis and pancreatic beta cells dysfunction through stimulating the IRE1alpha/TNF-alpha pathway and protective effect of taurine. Food Chem. Toxicol. : an international journal published for the British Industrial Biological Research Association 125, 392–402.

Qiu, T., Pei, P., Yao, X., Jiang, L., Wei, S., Wang, Z., et al., 2018. Taurine attenuates arsenic-induced pyroptosis and nonalcoholic steatohepatitis by inhibiting the autophagic-inflammasomal pathway. Cell Death Dis. 9 (10), 946–954.

Santhekadur, P.K., Kumar, D.P., Sanyal, A.J., 2018. Preclinical models of non-alcoholic fatty liver disease. J. Hepatol. 68 (2), 230–237.

Shan, B., Wang, X., Wu, Y., Xu, C., Xia, Z., Dai, J., et al., 2017. The metabolic ER stress sensor IRE1alpha suppresses alternative activation of macrophages and impairs energy expenditure in obesity. Nat. Immunol. 18 (5), 519–529.

Simao, A.L., Afonso, M.B., Rodrigues, P.M., Gama-Carvalho, M., Machado, M.V., Cortez-Pinto, H., et al., 2019. Skeletal muscle miR-34a/SIRT1:AMPK axis is activated in experimental and human non-alcoholic steatohepatitis. J. Mol. Med. 97 (8), 1113–1126.

Sorg, T.J., Chen, A.S., Wang, L., 2014. Arsenic species in drinking water wells in the USA

with high arsenic concentrations. Water Res. 48, 156–169.
Stockwell, B.R., Friedmann Angeli, J.P., Bayir, H., Bush, A.I., Conrad, M., Dixon, S.J., et al., 2017. Ferroptosis: a regulated cell death nexus linking metabolism, redox biology, and disease. Cell 171 (2), 273–285.
Thompson, C.B., 1995. Apoptosis in the pathogenesis and treatment of disease. Science (New York, NY) 267 (5203), 1456–1462.
Tsurusaki, S., Tsuchiya, Y., Koumura, T., Nakasone, M., Sakamoto, T., Matsuoka, M., et al., 2019. Hepatic ferroptosis plays an important role as the trigger for initiating inflammation in nonalcoholic steatohepatitis. Cell Death Dis. 10 (6), 449–454.
Wang, D., Shimoda, Y., Wang, S., Wang, Z., Liu, J., Liu, X., et al., 2017a. Total arsenic and speciation analysis of saliva and urine samples from individuals living in a chronic arsenicosis area in China. Environ. Health Prev. Med. 22 (1), 45–54.
Wang, P.X., Ji, Y.X., Zhang, X.J., Zhao, L.P., Yan, Z.Z., Zhang, P., et al., 2017b. Targeting CASP8 and FADD-like apoptosis regulator ameliorates nonalcoholic steatohepatitis in mice and nonhuman primates. Nat. Med. 23 (4), 439–449.
Wei, S., Qiu, T., Yao, X., Wang, N., Jiang, L., Jia, X., et al., 2019. Arsenic induces pancreatic dysfunction and ferroptosis via mitochondrial ROS-autophagy-lysosomal pathway. J. Hazard Mater. 384, 121390–121400.
Wenzel, S.E., Tyurina, Y.Y., Zhao, J., St Croix, C.M., Dar, H.H., Mao, G., et al., 2017. PEBP1 wardens ferroptosis by enabling lipoxygenase generation of lipid death signals. Cell 171 (3), 628–641.
Wu, J., Minikes, A.M., Gao, M., Bian, H., Li, Y., Stockwell, B.R., et al., 2019. Intercellular interaction dictates cancer cell ferroptosis via NF2-YAP signalling. Nature 572 (7769), 402–406.
Xie, Y., Hou, W., Song, X., Yu, Y., Huang, J., Sun, X., et al., 2016. Ferroptosis: process and function. Cell Death Differ. 23 (3), 369–379.
Yang, L., Chai, Y., Yu, J., Wei, B., Xia, Y., Wu, K., et al., 2017. Associations of arsenic metabolites, methylation capacity, and skin lesions caused by chronic exposure to high arsenic in tube well water. Environ. Toxicol. 32 (1), 28–36.
Yuan, H., Li, X., Zhang, X., Kang, R., Tang, D., 2016. Identification of ACSL4 as a biomarker and contributor of ferroptosis. Biochem. Biophys. Res. Commun. 478 (3), 1338–1343.